coatings

Article

# Synthesis and Frost Suppression Performance of PDMS-$SiO_2$/PFA Hybrid Coating

**Li Jia [1,2], Jun Sun [1,*], Xiaoxiao Li [1], Xian Zhang [1], Lin Chen [1] and Xinyou Tian [1,*]**

[1] Key Lab of Photovoltaic and Energy Conservation Materials, Institute of Solid State Physics, HFIPS, Chinese Academy of Sciences, Hefei 230031, China; jial2008@mail.ustc.edu.cn (L.J.); lixiaoxiao@rntek.cas.cn (X.L.); xzhang@issp.ac.cn (X.Z.); chenlin@issp.ac.cn (L.C.)

[2] University of Science and Technology of China, Hefei 230026, China

* Correspondence: jsun@rntek.cas.cn (J.S.); xytian@issp.ac.cn (X.T.); Tel.: +86-551-65393564 (J.S.); +86-551-65591418 (X.T.)

**Abstract:** In this article, a simple synthesis method was applied to form a branch and tendril structure using hydroxyl-terminated silicone sol modified silica nanoparticles at high temperature, followed by mixing with fluoro-containing polyacrylate emulsion (PFA) to obtained a polydimethylsiloxane (PDMS)-$SiO_2$/PFA hybrid coating. The hydrophobic performance of the PDMS-$SiO_2$/PFA coating was further enhanced through the synergistic action of Si-O and F group. The obtained coating has a similar surface structure of lotus leaf and the contact angle can reach 142.2 ± 2.4°. The PDMS-$SiO_2$/PFA coating could delay the formation of frost crystal and the growth of frost layer. The defrosting droplets were difficult to adhere on the coating and could be easily rolled off for long frosting and defrosting cycles, which indicates the potential application of this coating in the field of frost suppression.

**Keywords:** $SiO_2$; nanoparticles; hydrophobic coating; anti-frosting



**Citation:** Jia, L.; Sun, J.; Li, X.; Zhang, X.; Chen, L.; Tian, X. Synthesis and Frost Suppression Performance of PDMS-$SiO_2$/PFA Hybrid Coating. *Coatings* **2021**, *11*, 256. https://doi.org/10.3390/coatings11020256

Received: 28 December 2020
Accepted: 18 February 2021
Published: 22 February 2021



## 1. Introduction

Nowadays, frosting on cold surfaces has received widespread concern in refrigerators owing to the new energy consumption national standard requirements. The first study on the phenomenon of free flow condensation and frosting on pipes was conducted by Pienning [1] in Germany in the 1830s. Since then, numerous methods have been developed including frost suppression techniques. These techniques can be classified into three types: (1) reducing the ambient air humidity; (2) using the extra field energy to change the form of droplet freezing and frost crystal formation followed by inhibiting the growth of frost layer; and (3) surface modification. However, air humidity should be maintained at a certain level to ensure its function in many practical applications such as in refrigerators, while the external field is limited by space limitations and equipment complexity. Compared with the above defrosting technologies, surface modification was one of the most promising approaches to anti-frost because of its simplicity and lower cost.

As one of the most promising surface modification methods, hydrophobic surfaces have attracted great interest of many researchers because of their advantages of energy saving and simplicity. Hydrophobic surfaces could reduce the retention of water droplets on the surface [2], delay the freezing time of water droplets [3–6], and reduce the adhesion between ice and the surface [7–11]; these aspects have attracted the interests of researchers. In previous studies, much attention has been paid to the hydrophobic surface obtained by mechanical process. For example, Ogawa et al. [12,13] constructed a micron-nano structure on the substrate surface using the etching method, and the contact angle could increase above 150°. Wang et al. [14] constructed micro-nano structures on the aluminum surface by acid etching, and then modified them with a fluorine-containing coupling agent, silane coupling agent, and hexadecanoic acid to form three kinds of superhydrophobic surfaces.

They also studied the anti-icing efficiency of the three hydrophobic surfaces. Emelyanenko et al. [15] prepared hydrophobic and superhydrophobic silicone rubber surfaces by laser etching. The results showed that the superhydrophobic surface modified with fluorosilane exhibited better hydrophobic stability and anti-icing performance. Guo et al. [16] and Mishchenko et al. [17] prepared a micron structure on the base surface and studied its ice-resistance performance. However, the mechanical process has many defects, such as the limiting shape of the parts, high cost, complex operation, and so on. Hence, it is necessary to find an effective method to achieve practical applications.

Numerous methods, i.e., plasma etching, electrospinning, and the template method, have been reported to structure the superhydrophobic surface. In most studies, the polymer, such as polyacrylate, polydimethylsiloxanes, polyaniline, and so on, is used as a low surface energy material to fabricate the superhydrophobic surface. Compared with other polymers, polydimethylsiloxane (PDMS) is used extensively in coating industries because of its unique and flexible structure, durable performance, good biological compatibility, and low cost. Therefore, many preliminary studies have been carried out on PDMS for frost/ice suppression; for example, Wang [18] synthesized super durable PDMS/ZnO hydrophobic coating using the template method. They found that the hydrophobic performance did not decrease obviously after hundreds of repetitions of icing–deicing cycles and bending tests. However, the template method was restricted by the size of the template to construct a nano-micro structure, so it is difficult to produce in large scale. Yeong et al. [19] and Wang [20] synthesized the anti-icing surface of organic gel with lubricant to improve the durability in the process of icing/deicing using PDMS as the skeleton, but the organic solvent is not suitable for practical production because of its high price, toxicity, and environmental unfriendliness. Fluorinated polyacrylate is one of the most promising materials for the preparation of hydrophobic materials owing to its corrosion resistance, optical transparency, excellent mechanical properties, and better weather resistance [21–24]. Meanwhile the fluorine chain can provide low surface energy and the acrylic group has good adhesion on a variety of substrate materials, but there are few reports on the frost inhibition of fluorinated polyacrylate.

Compared with the old energy efficiency standard, the energy consumption of a new refrigerator for one level needs to increase by about 14%, while the frosting–defrosting process would contribute to about a 3~5% decrease. However, it is still a challenge to defrost on various substrates, such as metal and plastic, in a refrigerator. In this paper, a simple method was applied to prepare hydrophobic material using hydroxyl-terminated silicone modified with silica nanoparticles at a high temperature, and further mixing the nanoparticles with fluoro-containing polyacrylate (PFA) to yield a PDMS-$SiO_2$/PFA emulsion. The emulsion could form a stable coating on a variety of substrate materials owing to the good adhesion of the acrylate group. The hybrid coatings were characterized by scanning electron microscope (SEM), transmission electron microscopy (TEM), energy dispersive spectroscopy (EDS), Fourier transform infrared (FTIR) spectra, and water contact angle (WCA), and the effect of anti-frost on the evaporator was also investigated. The as-prepared coating has a close superhydrophobic property; meanwhile, its anti-frost effect does not decrease obviously after more than 2800 min of frosting and defrosting cycles.

## 2. Materials and Methods

### *2.1. Materials*

Hydrophobic nano-silica particles (diameter of 16–20 nm) were purchased from Xinhong Chemical Co., Ltd. (Taicang, China); polydimethylsiloxanes (PDMS400, industrial products) were purchased from Foshan Vago Organic Silicon Co., LTD. (Foshan, China); dodecafluoroheptyl methacrylate (FMA, A. R.) was supplied by XEOGIA Fluorine-Silicon Chemical Co., Ltd. (Harbin, China). Methyl methacrylate (MMA, A. R.), butyl acrylate (BA, A. R.), acrylic acid (AA, A. R.), acetone (A. R.), potassium persulfate (KPS, A. R.), sodium lauryl sulfate (SDS), and alkylphenol polyoxyethylene ether (OP-10) were purchased from

Sinopharm Chemical Reagent Co., Ltd. (Shanghai, China). All the reagents were used as received.

### 2.2. Synthesis of PDMS-$SiO_2$ Hybrid and PFA Emulsion

PDMS and $SiO_2$ were heated at 110 °C in a vacuum oven for 8 h. Then, PDMS and $SiO_2$ with a mass ratio of 2.5 to 20.5 and anhydrous calcium chloride (as desiccant) were put into a Teflon-lined autoclave, sealed under nitrogen atmosphere, and heated at 180 °C for more than 10 h to react completely. The PDMS-$SiO_2$ nano-particles were repeatedly washed using acetone followed by vacuum filtration. The filtrate cake was then put in an oven and heated at 70 °C for 10 h to obtain the PDMS-$SiO_2$.

The PFA emulsion was synthesized using two-stage technology. At the first stage, MMA, BA, AA, and FMA were mixed into a beaker with the weight ratio of 20:30:0.8:8 under vigorously magnetic stirring. Then, KPS, SDS, OP-10, and water were mixed with the weight ratio of 0.2:0.4:1.6:87. At the second stage, the above product was mixed and stirred for more than 1 min followed by ultrasonic emulsification. Then, 40 mL pre-emulsion was added into a four-necked flask and stirred with 3000 rpm for 1 h at 80 °C until the mixture turned light blue. Next, the remaining pre-emulsion was added dropwise into the above emulsion solution under agitation. Finally, the fluorine-containing polyacrylate emulsion was obtained after reaction for another 2 h.

### 2.3. Synthesis of PDMS-$SiO_2$/PFA Hybrid Coating

PDMS-$SiO_2$ nano-particles and ethanol (a mass ratio of 1:10) were mixed in a clean beaker with vigorously magnetic stirring. Then, different amounts of PFA were added to the stirred dispersion and the resulting mixture was ultrasonicatied for another 15 min. Finally, the PDMS-$SiO_2$/PFA hybrid coating was fabricated on the sample piece through the brush process, and the coating samples were placed in an oven at 70 °C for 5 h to promote solvents' volatilization and film forming.

### 2.4. Film Thickness and Adhesion Test

The test method of film thickness and adhesion concerning the as-prepared PDMS-$SiO_2$/PFA hybrid coating (with mass ratio of PDMS-$SiO_2$ to PFA of 0.5) on the aluminum substrate refers to GB/T 9286-1998 paints and varnishes cross cut test for films. First, a vertical intersecting grid was cut on the coating surface with a hundred grid knife, then the scattered particles were removed with a brush, and the adhesion characteristics of the coating grid with 3M 600 transparent tape were tested. Finally, a magnifying glass was used to observe the cutting area of the coating. The above experiments were repeated at least three times. The whole set testing tools were purchased from Dongguan Quick Measuring Instrument Co., LTD (Dongguan, China).

### 2.5. Frosting Test

The frosting tests were performed on a refrigerator evaporator pipe of BCD-171SQMK (MIDEA, Hefei, China). The PDMS-$SiO_2$/PFA hybrid coating was fabricated onto the surface of the evaporator pipe by brush. For comparison, the frost test was performed on the same evaporator pipe, where half of the evaporator pipe was brushed with PDMS-$SiO_2$/PFA hybrid coating while the other half was not treated. During the test, a microsquare camera monitoring system was utilized to capture the process of frosting and defrosting on the evaporator pipe.

### 2.6. Characterization

Micro morphology observations were taken with a transmission electron microscopy (TEM) instrument (JEM-2010, JEOL, Tokyo, Japan) at an acceleration voltage of 200 KV. The sample solution was placed on the copper grid and dyed by phosphotungstic acid, and dried in air before observation. Scanning electron microscopy (SEM) images were examined with a Sirion 200 field-emission scanning electron microscopy (SEM, Sirion 200, FEI, Hillsboro, OR, USA), and element analysis was performed with an energy dispersive spectroscopy (EDS) unit from SEM. The Fourier transform infrared (FTIR) spectra (NEXUS-870, Nicolet Instrument Co., Madison, WI, USA) were recorded in the range of 400–4000 $cm^{-1}$. The coating samples were dispersed into KBr, then ground to pieces with mortar, and finally pressed into tablets for FTIR testing. Water contact angle (WCA) was determined by a contact angle analyzer (KRUSS DSA10Mk2, Hamburg, Germany) with 5 μL distilled water. The roll-off angles of the drops were measured by a contact angle analyzer (INNUO CA100D, shanghai, China) and the pictures were recorded by the optical CCD of the system. Digital images were taken by a digital single lens reflex camera (Sony, Tokyo, Japan). The process of frosting and defrosting on the evaporator pipe was recorded by the software of a microsquare camera monitoring system.

## 3. Results and Discussion

### *3.1. Surface Topography*

TEM images of PDMS modified $SiO_2$ and PDMS-$SiO_2$/PFA with mass ratio of PDMS-$SiO_2$ to PFA of 0.5 are shown in Figure 1. It is clear that the $SiO_2$ nanoparticles overlapped with each other to form a branch and tendril structure. The single PDMS-$SiO_2$ particle size was about 20 nm and the aggregating size was 50–120 nm, which was consistent with our previous study [25]. As shown in Figure 1b, PFA has a good coating effect on PDMS-$SiO_2$ particles, which causes the particles to agglomerate together. SEM images of PDMS-$SiO_2$ and PDMS-$SiO_2$/PFA are shown in Figures 2 and 3, respectively. There were many island-like convex structures on the PDMS-$SiO_2$ surface. According to the EDS (Figure 2c), the PDMS-$SiO_2$ particles were mainly composed of C, Si, and O elements, and the atom percentages were about 27%, 17%, and 56%, respectively. The element atom ratio of C in the particles confirmed that the grafting reaction on the $SiO_2$ surface was successful [25]. Then, the PDMS-$SiO_2$ particles were tightly attached to each other by the adhesive action of PFA after mixing with PFA emulsion [21]. The observed rough surface, as shown in Figure 3, exhibits many mountain-like bulges that are similar to the surface structure of lotus leaf (Figure 3b). The protrusions were composed of PDMS-$SiO_2$ particles with different sizes from nanoscale to microscale that could form the binary nano-micro structure. The main reason is that the surface of the $SiO_2$ particles is modified by hydrophobic PDMS and has a branch structure. In the drying process of the coating, hydrophobic PDMS-$SiO_2$ particles are relatively easy to agglomerate on the surface of the coating, and PFA displays good polymer coating performance, which can effectively agglomerate the particles together and provide excellent coating adhesion. Finally, the PDMS-$SiO_2$/PFA hybrid coating with similar surface morphology to lotus leaf was obtained. As shown in the EDS image (Figure 3c), the PDMS-$SiO_2$/PFA hybrid coating was mainly composed of C, Si, O, and F elements, and the atom percentages were about 35%, 19%, 45%, and 1%, respectively. The appearance of C, Si, and F elements indicated that PDMS and PFA with low surface free energy are successfully introduced into the hybrid coating.

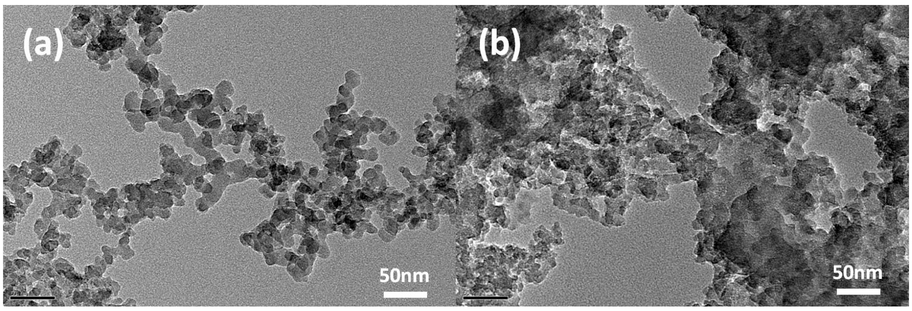


**Figure 1.** Transmission electron microscopy (TEM) image of (**a**) polydimethylsiloxane (PDMS)-$SiO_2$ and (**b**) PDMS-$SiO_2$/PFA with a mass ratio of PDMS-$SiO_2$ to PFA of 0.5.

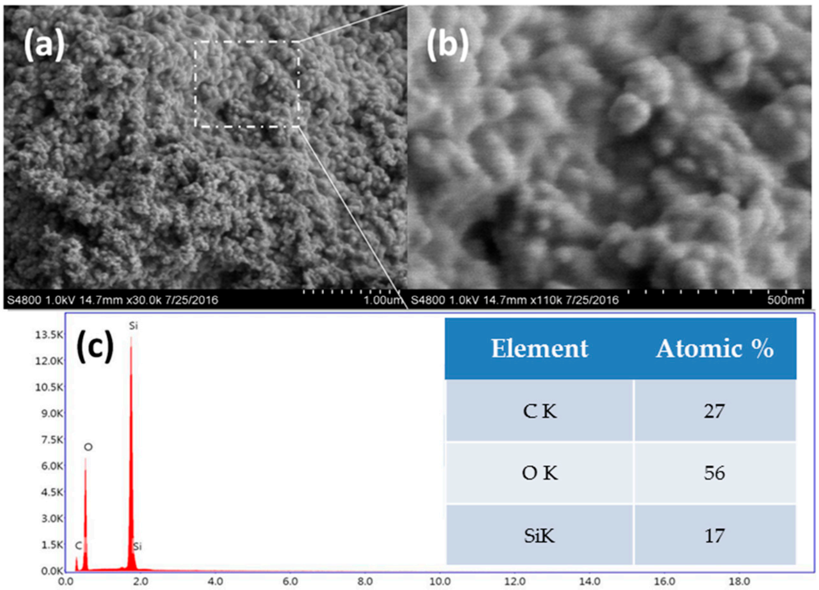


**Figure 2.** (**a**,**b**) Scanning electron microscopy (SEM) images of PDMS-$SiO_2$. (**c**) Energy dispersive spectroscopy (EDS) image of PDMS-$SiO_2$.

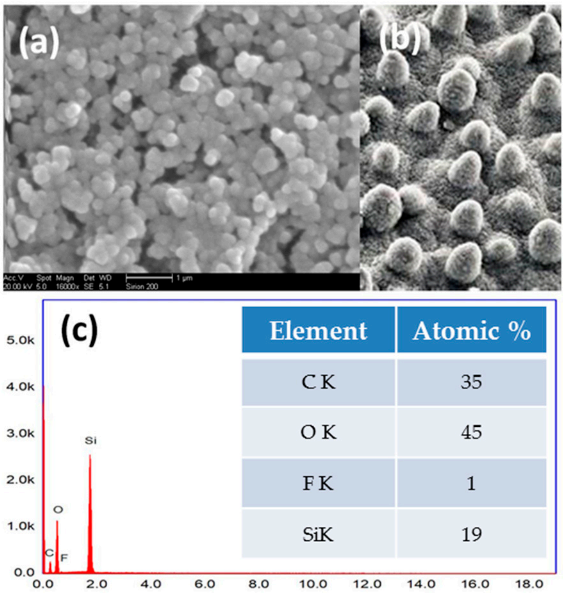


**Figure 3.** SEM images of (**a**) PDMS-$SiO_2$/PFA coating with a mass ratio of PDMS-$SiO_2$ to PFA of 0.5 and (**b**) lotus leaf surface. (**c**) EDS image of PDMS-$SiO_2$/PFA coating with a mass ratio of PDMS-$SiO_2$ to PFA of 0.5.

### *3.2. FTIR*

The FTIR spectra of the PDMS-$SiO_2$ and PDMS-$SiO_2$/PFA coatings are shown in Figure 4. Typical absorption peaks at 1265 $cm^{-1}$ (Si-$CH_3$), 1078 $cm^{-1}$, 1016 $cm^{-1}$ (Si-O-Si), and 803 $cm^{-1}$ ($CH_3$-Si) [26] could confirm that the PDMS chain segment has been successfully introduced into the surface of $SiO_2$. According to the spectrum of PDMS-$SiO_2$/PFA, the peaks at 2968 $cm^{-1}$, 2875 $cm^{-1}$, and 1447 $cm^{-1}$ were assigned to the C-H bond (-$CH_2$, -$CH_3$) stretching vibrations of the polymer chain, while the peak at 1731 $cm^{-1}$ was assigned to the C=O stretching vibrations. Meanwhile, the characteristic absorption peak of the C-F bond in –$CF_3$ at 667 $cm^{-1}$ and the bending vibration peaks of -$CF_2$ and –CF at 794 $cm^{-1}$ indicated the successful introduction of F groups into PFA [27,28]. Moreover, the typical absorption peaks of Si-C-$H_3$, Si-O-Si, and $CH_3$-Si appeared in the spectra of the

PDMS-$SiO_2$/PFA composite sample could confirm that the siloxane group of PDMS-$SiO_2$ was successfully introduced into the PFA emulsion [29].

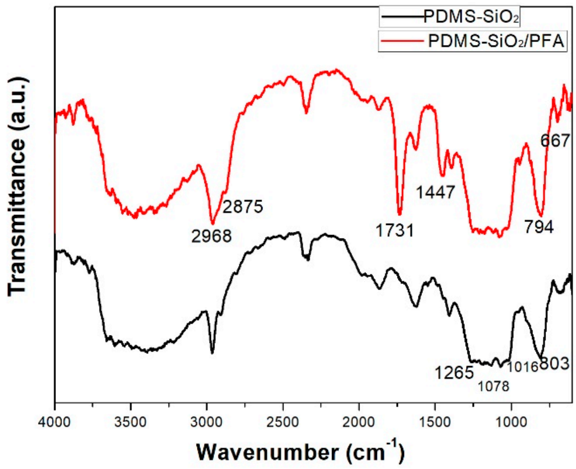


**Figure 4.** Fourier transform infrared (FTIR) spectra of PDMS-$SiO_2$ and PDMS-$SiO_2$/PFA with a mass ratio of PDMS-$SiO_2$ to PFA of 0.5.

### 3.3. Surface Wettability

The WCAs of PDMS-$SiO_2$/PFA hybrid coatings with different PDMS-$SiO_2$ content are shown in Figure 5b. PFA film without PDMS-$SiO_2$ nanoparticles has a WCA of 42.6 $\pm$ 2.1°, which was hydrophilic. After introducing PDMS-$SiO_2$ nanoparticles into the film, the WCAs of PDMS-$SiO_2$/PFA hybrid coatings increased significantly at first and then reached a constant value with the increasing of PDMS-$SiO_2$. When the content of PDMS-$SiO_2$ was 0.2, the WCA of the hybrid coating was 129.6 $\pm$ 1.8°, showing that the hydrophobic performance of the as-prepared coating was significantly improved by the introduction of PDMS-$SiO_2$ particles. When the content of PDMS-$SiO_2$ was 0.3, the WCA of PDMS-$SiO_2$/PFA was about 134.8 $\pm$ 1.5°. However, when the content of the PDMS-$SiO_2$ further increased to 0.5, the WCA slightly increased to 142.2 $\pm$ 2.4°. However, demulsification occurred in the mixed solution when more nanoparticles were added. This may be caused by the high PDMS-$SiO_2$ content; the high content may have an adverse effect on the PFA emulsion stability and the dispersion in the PFA. The result showed that the amount of PDMS-$SiO_2$ is a critical factor affecting the surface roughness and wettability of the hybrid coating. Briefly, a suitable amount of PDMS-$SiO_2$ will produce better surface roughness (SEM). The dispersion was poor and the aggregation could occur at a high amount of PDMS-$SiO_2$. In this study, the maximum value of PDMS-$SiO_2$ content was about 0.5.

It is well known that the construction of a micro-nano structure and the introduction of low surface free energy are the two key methods for the preparation of hydrophobic surfaces [30–32]. For PDMS-$SiO_2$/PFA hybrid coatings, PDMS-$SiO_2$ nanoparticles are cross-linked with each other through the hydrophobic chain of PDMS, which further leads to the increase of clusters with different sizes, and then the micro-nano structure (Figure 2) is formed, and the surface become more hydrophobic with the increase of surface roughness [33,34]. On the other hand, holes would be formed between the clusters (Figure 1). This structure could form a solid–air–water contact mode and further enhance the hydrophobic performance [31,34]. Besides, element F and organic silicon (PDMS) group could introduce low-surface free energy groups on the surface of silica, and the synergistic effect can further improve the hydrophobic performance [27,28].

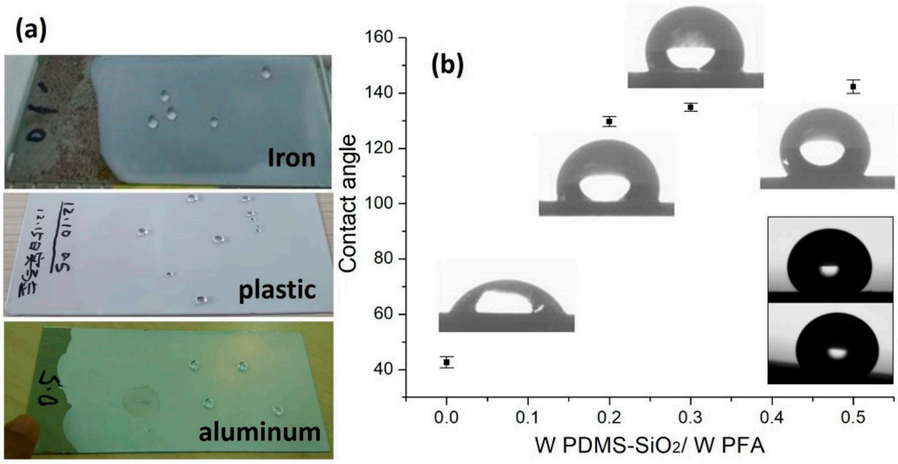


**Figure 5.** (**a**) Fabrication of hydrophobic PDMS-$SiO_2$/PFA coating on iron, aluminum, and plastic substrates; (**b**) water contact angles (WCAs) of PDMS-$SiO_2$/SS hybrid coating on aluminum substrate with different mass ratio of PDMS-$SiO_2$ to PFA. The picture in the lower right corner of figure (**b**) is of the roll-off angle test.

The PDMS-$SiO_2$/PFA sample could construct a hydrophobic surface on various substrates because of the good adhesion of the acrylate group [21–23] in iron, aluminum, and plastic substrates, as shown in Figure 5a. The water droplets presented a spherical shape, which could confirm that the coating had good hydrophobicity. The roll-off angle of the as-prepared PDMS-$SiO_2$/PFA hybrid coating on the aluminum substrate is 7.34 ± 0.39° (Figure 5). As shown in Video S (supporting information Video S), water droplets roll off easily from the surface of the as-prepared PDMS-$SiO_2$/PFA coating when inclined at a small angle, indicating that the coating had a low rolling angle.

The thickness and adhesion of the as-prepared PDMS-$SiO_2$/PFA hybrid coating (with a mass ratio of PDMS-$SiO_2$ to PFA of 0.5) on the aluminum substrate were tested referring to GB/T 9286-1998 paints and varnishes cross cut test for films. The average thickness of this film is 0.0627 mm. As shown in Figure 6, the adhesion of the film was measured by the cross cut test. When the coating is cross cut, the coating surface of the grid is basically intact. After adhesion and stripping with 3M 600 transparent tape, a little coating fell off at the intersection of the incisions, and the affected coating area was obviously less than 15%. According to the GB/T 9286-1998 paints and varnishes cross cut test for films, the adhesion of the as-prepared PDMS-$SiO_2$/PFA hybrid coating can reach grade II.

### *3.4. Frosting Characteristics*

In order to investigate the anti-frosting performance of PDMS-$SiO_2$/PFA hybrid coatings, the dynamic frost process on refrigerator evaporator aluminum pipe was carried out. For comparison, half of the evaporator pipe was treated with PDMS-$SiO_2$/PFA hydrophobic coating with mass ratio of PDMS-$SiO_2$ to PFA of 0.5, and the other half remained untreated. The working temperature and humidity in the refrigerator were basically stable at −20.5 °C and 40.1% relative humidity (RH), respectively, and the surface temperature of the evaporator was maintained at −30.2 °C. During the test, a microsquare camera monitoring system was used to record the process of frosting and defrosting.

The coating could delay the frost crystal appearing time by about 186 min, according to Figure 7. After 114 min, the frost crystals appeared on the uncoated evaporator surface. However, after about 300 min, the needle-like frost crystal began to appear on the hybrid coating surface. With the extension of the testing time, the frost layer on the uncoated section of evaporator was thicker and the adhesive strength was enhanced. The frost layer on the coated section was thinner and could be removed easily with a gently sweep after 467 min (Figure 8). The reason may be that the PFA in PDMS-$SiO_2$/PFA coating could absorb moisture to form an aqueous lubrication layer, the layer could reduce the frost adhesion on the surface of the evaporator, and hence the frost could be easily removed by external force [35]. The experimental results revealed that the frosting starting time on the PDMS-$SiO_2$/PFA coating surface is obviously delayed compared with that on the uncoated section surface. Further, the inhibition of the frost layer during the whole frosting process on the coating surface is also significantly improved compared with that on the uncoated section surface. Frosting on a cold surface is a typical phase transition that should overcome the potential barrier. According to the previous research, increasing the contact angle is one critical factor for improving the potential barrier [36]. In this study, the contact angle of PDMS-$SiO_2$/PFA hybrid coated surface was 142.2 $\pm$ 2.4°, while the uncoated surface was about 42.6 $\pm$ 2.1° (Figure 5). Hence, the potential barrier was much higher than that of the uncoated surface. Consequently, the time of the appearance of frost crystal nucleation and the frost growth process on the coating surface is enhanced compared with the uncoated surface.

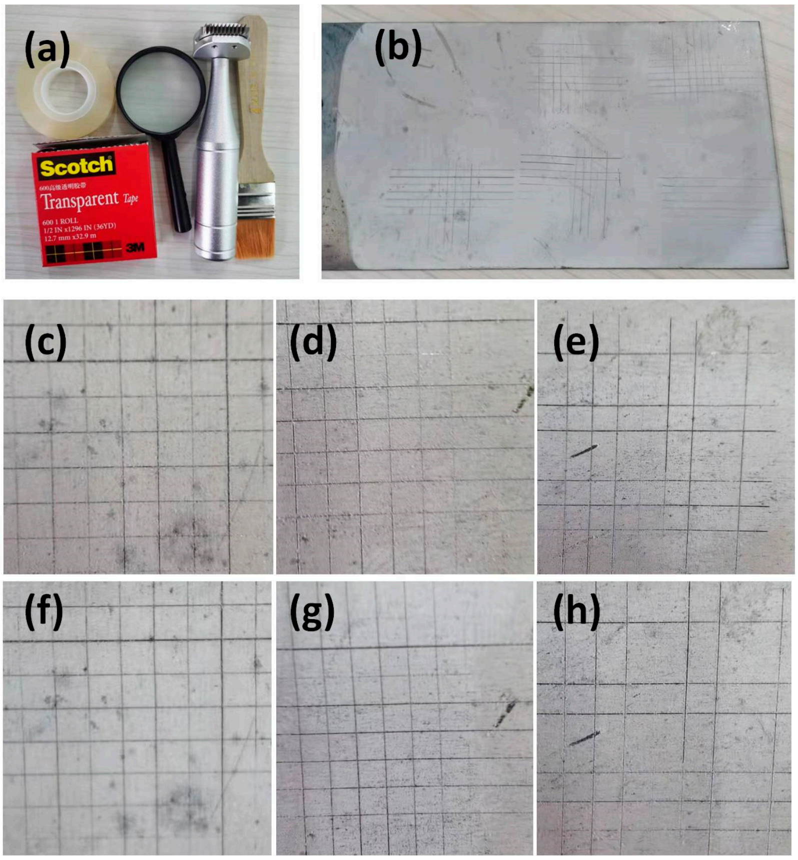


**Figure 6.** (**a**) Adhesion testing tool. (**b**) The sample of PDMS-$SiO_2$/PFA hybrid coating on the aluminum substrate for the test. (**c**–**e**) The surface diagrams of three different regions after cross cut. (**f**–**h**) The surface diagrams of three different regions after adhesion and stripping with 3M 600 transparent tape corresponding to (**c**–**e**).

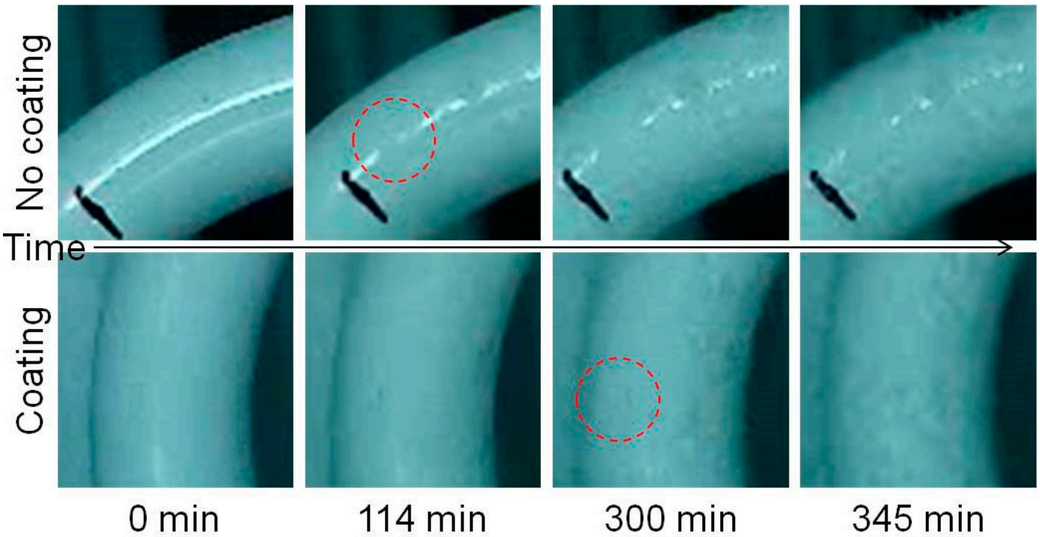


**Figure 7.** Frost formation process and variation of frost mass with different times for various surfaces: normal surfaces and PDMS-$SiO_2$/PFA hybrid coating surfaces.

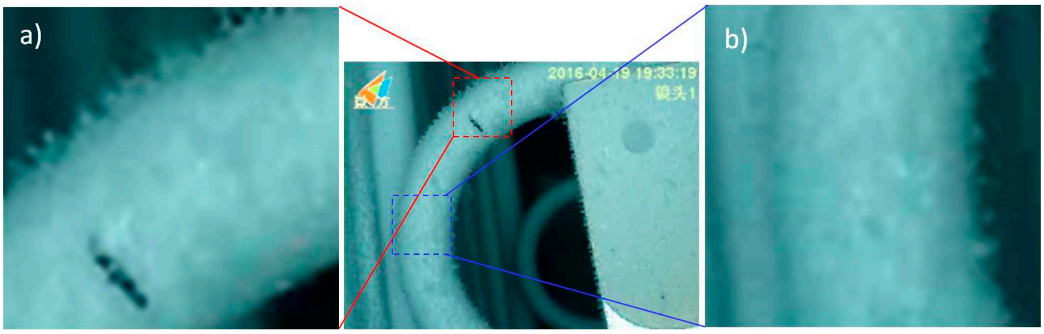


**Figure 8.** Frost formation process and variation of frost mass after 467 min with different surface conditions: (**a**) normal surfaces; (**b**) PDMS-$SiO_2$/PFA hybrid coating surfaces. Note: 微方 is a brand and 镜头1 means camera No.1.

In order to verify the anti-frosting performance of the PDMS-$SiO_2$/PFA hybrid coating, the defrosting and frosting processes were placed on the same evaporator. As shown in Figure 8, it can be observed that the melt frost droplets were difficult to adhere on the coating part owing to low surface free energy, and the residual small droplets could coalesce with each other and jump off the surface easily [37]. Therefore, there is only a thin frost layer on the coating surface in the frost process until the next frost cycle begins. In contrast, the melt frost water spread into filmwise and dropwise condensation with hemisphere shape on the uncoated section surface. The melt frost droplets provided most of the frosting crystal points that accelerated the frost process on the next experiment cycles (Figures 9 and 10). The experiment results indicated that the evaporator with PDMS-$SiO_2$/PFA hybrid coating displayed better anti-frosting property than the uncoated section under the same conditions. The anti-frosting performance remained almost unchanged after the secondary cycle, and no significant decrease occurred. This may be attributed to the unique flexibility of PDMS in the hybrid coating under the certain deformation, resulting in the relative volume change in the frosting and defrosting process [17], which can improve the durability of hydrophobic coating. In order to verify the frost suppression stability of the PDMS-$SiO_2$/PFA hybrid coating, the refrigerator worked continuously for more than 2800 min (more than ten frosting and defrosting cycles), and the dynamic frost formation process on the evaporator pipe surface was observed by a digital single lens reflex (SLR) camera at different times. As shown in Figure 11, the defrosting water converges into many filmwise and dropwise droplets on the surface of the evaporator without coating. In contrast, only a few defrosting droplets appear on the surface of the evaporator pipe with the as-prepared PDMS-$SiO_2$/PFA hybrid coating. Furthermore, the amount of frost on the evaporator pipe surface with PDMS-$SiO_2$/PFA hybrid coating decreased significantly compared with the evaporator pipe surface without coating during the whole frosting and defrosting cycles. Generally, the as-prepared PDMS-$SiO_2$/PFA hybrid coating can effectively improve the anti-frosting performance of the evaporator pipe surface for a long time. During the test, the working temperature and humidity in the refrigerator were basically stable and corresponded to T= −20.5 °C and 40.1% RH, respectively, while the surface temperature of the evaporator was maintained at −30.2 °C. Taking into account the variation of the water vapor pressure with temperature [38], it is easy to estimate that the humidity of the ice vapor in the refrigerator with respect to the surface of the evaporator was about RH = 106%. Therefore, the obtained supersaturation, allowing suppression of frost formation, is smaller than that achieved in [39], indicating the necessity of further improving the properties of the coating. At the same time, the obtained results allow getting an optimistic view on the strategy suggested in our study. It is obvious that this PDMS-$SiO_2$/PFA coating is useful for the design of the hydrophobic coating, and the PDMS-$SiO_2$/PFA coating also has potential applications in the field of anti-frost, especially in these products containing a variety of base materials, e.g., a refrigerator.

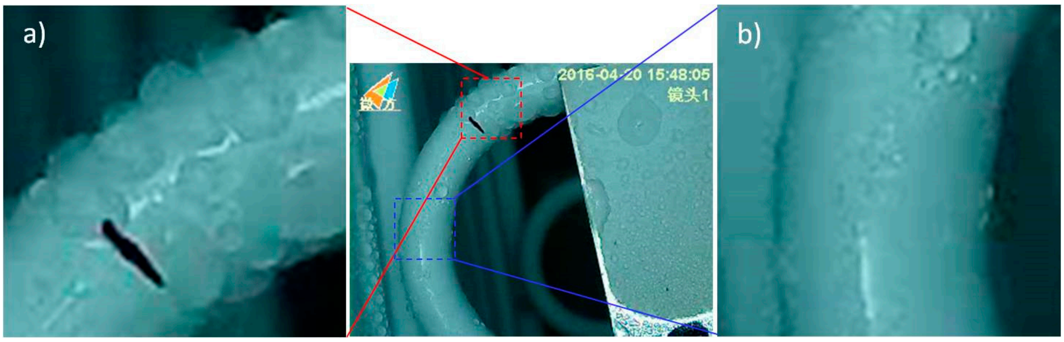


**Figure 9.** Condensation of defrost droplets on the evaporator with different surface conditions: (**a**) normal surfaces; (**b**) PDMS-$SiO_2$/PFA hybrid coating surfaces. Note: 微方 is a brand and 镜头1 means camera No.1.

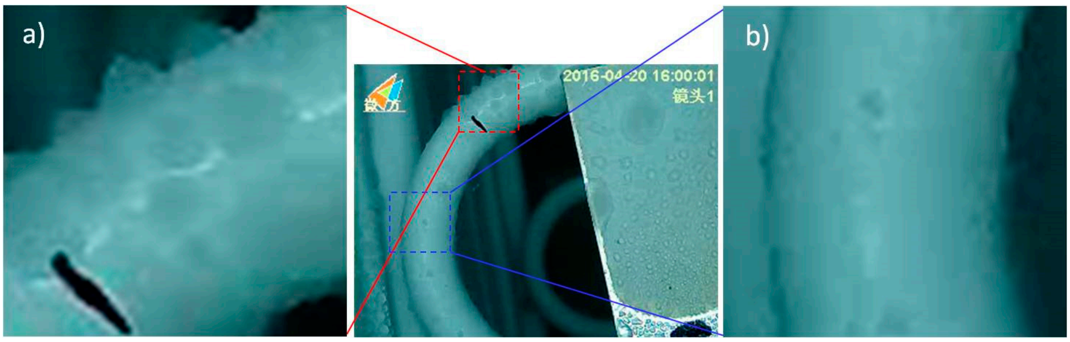


**Figure 10.** Frost formation process with different surface conditions: (**a**) normal surfaces; (**b**) PDMS-$SiO_2$/PFA hybrid coating surfaces. Note: 微方 is a brand and 镜头1 means camera No.1.

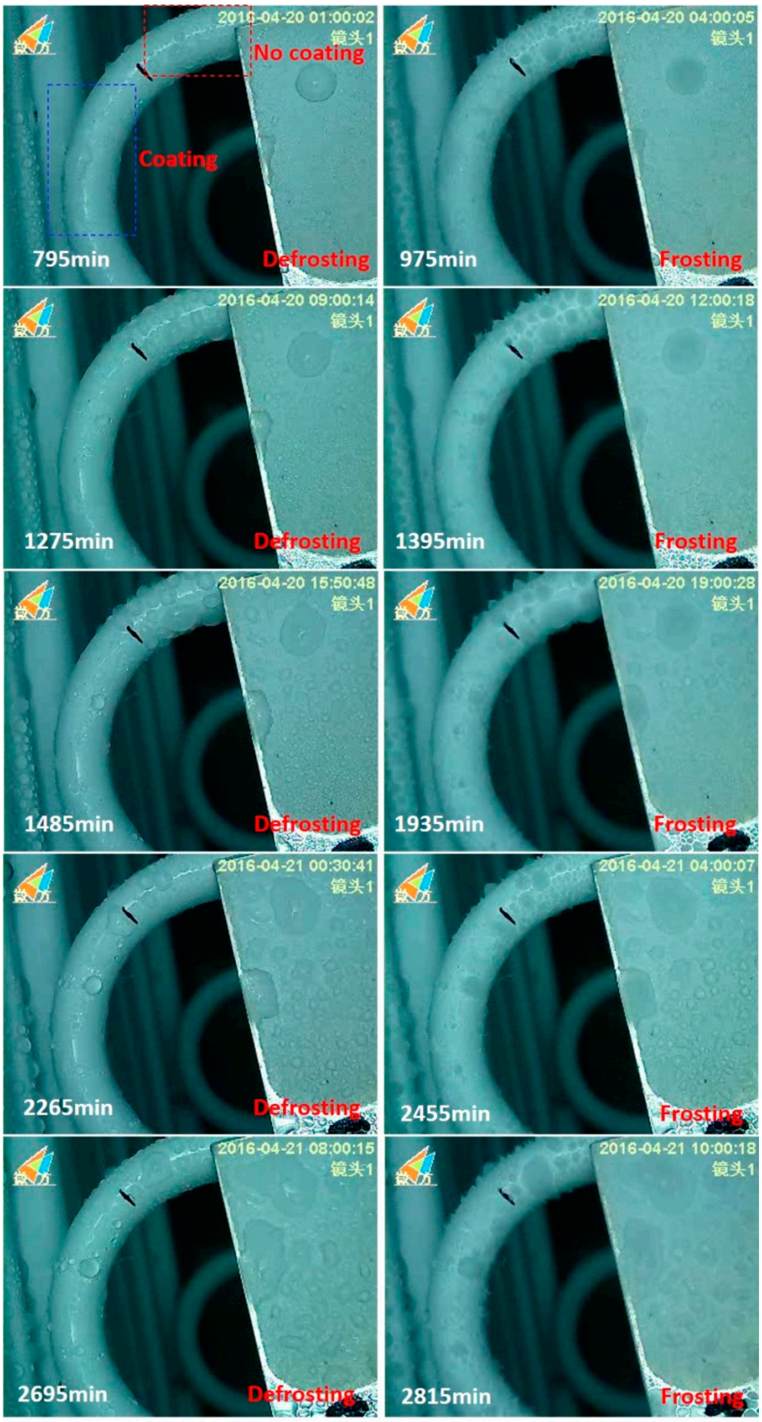


**Figure 11.** Frosting and defrosting cycles with time on the surface of the evaporator pipe without and with the PDMS-$SiO_2$/PFA hybrid coating. Note: 微方 is a brand and 镜头1 means camera No.1.

## 4. Conclusions

Hydrophobic PDMS-$SiO_2$ nanoparticles could construct a lotus structure on the substrate surface. The content of PDMS-$SiO_2$ in the hybrid coating was a critical factor for the hydrophobic performance. The WCA of PDMS-$SiO_2$/PFA coating with 0.5 PDMS-$SiO_2$ content could reach up to $142.2 \pm 2.4°$, which is close to super-hydrophobic property. The coating can construct a hydrophobic surface on various substrates owing to the good adhesion of the acrylate group. The frosting results showed that the PDMS-$SiO_2$/PFA hybrid coating on the evaporator not only effectively enhanced the frost crystal time, but also reduced the growing speed of the frost layer compared with the no-coating evaporator surface. The defrosting droplets could not easily adhere on the coating and could easily roll off from the coating. Furthermore, the defrosting performance of the coating did not decrease significantly after more than 2800 min of frosting and defrosting cycles. This implies that the as-prepared PDMS-$SiO_2$/PFA hybrid coating on the evaporator has a better anti-frosting performance, thus providing a good guidance for frost suppression of refrigerators in the home appliance industry.

**Author Contributions:** L.J.: conceptualization, methodology, investigation, data curation, writing—original draft preparation. J.S.: conceptualization, methodology, investigation, data curation, writing—original draft preparation, writing—review and editing, funding acquisition. X.L.: methodology, writing—review and editing, funding acquisition. X.Z.: methodology, writing—review and editing, funding acquisition. L.C.: conceptualization, data curation, writing—review and editing, funding acquisition. X.T.: conceptualization, writing—review and editing, funding acquisition. All authors have read and agreed to the published version of the manuscript.

**Funding:** This research is funded by the National Key Research and Development Program of China under 2017YFC0703200 and Youth Innovation Promotion Association, CAS (2015268).

**Data Availability Statement:** Data is contained within the article.

**Acknowledgments:** All the coauthors thank Key Lab of Photovoltaic and Energy Conservation Materials, Chinese Academy of Sciences. All the authors thank Hefei Midea refrigerator Co. Ltd. for their support in the refrigerator experiment.

**Conflicts of Interest:** The authors declare no conflict of interest.

## References


1. Piening, W. The heat transfer-on tubes with free flow taking into account the formation of condensation and mature. *Health Eng.* **1933**, *56*, 493–501.
2. Jung, S.; Tiwari, M.K.; Doan, N.V.; Poulikakos, D. Mechanism of supercooled droplet freezing on surfaces. *Nat. Commun.* **2012**, *3*, 615–623. [CrossRef]
3. Xu, Q.; Li, J.; Tian, J.; Zhu, J.; Gao, X.F. Energy-effective frost-free coatings based on superhydrophobic aligned nanocones. *ACS Appl. Mater. Interfaces* **2014**, *6*, 8976–8980. [CrossRef]
4. Ruan, M.; Li, W.; Wang, B.S.; Deng, B.W.; Ma, F.M.; Yu, Z.L. Preparation and anti-icing behavior of superhydrophobic surfaces on aluminum alloy substrates. *Langmuir* **2013**, *29*, 8482–8491. [CrossRef] [PubMed]
5. Hu, Z.Y.; Zhang, X.M.; Liu, Z.Y.; Huo, K.F.; Chu, P.K.; Zhai, J.; Jiang, L. Regulating water adhesion on superhydrophobic $TiO_2$ nanotube arrays. *Adv. Funct. Mater.* **2014**, *24*, 6381–6388. [CrossRef]
6. Wang, L.; Wen, M.X.; Zhang, M.Q.; Jiang, L.; Zheng, Y.M. Ice-phobic gummed tape with nano-cones on microspheres. *J. Mater. Chem. A* **2014**, *2*, 3312–3316. [CrossRef]
7. Croutch, V.K.; Hartley, R.A. Adhesion of ice to coatings and the performance of ice release coatings. *J. Coat. Technol.* **1992**, *64*, 41–53.
8. Bharathidasan, T.; Kumar, S.V.; Bobji, M.S.; Chakradhar, R.P.S.; Basu, B.J. Effect of wettability and surface roughness on ice-adhesion strength of hydrophilic, hydrophobic and superhydrophobic surfaces. *Appl. Surf. Sci.* **2014**, *314*, 241–250. [CrossRef]
9. Ling, E.J.Y.; Uong, V.; Renault-Crispo, J.S.; Kietzig, A.M.; Servio, P. Reducing ice adhesion on nonsmooth metallic surfaces: Wettability and topography effects. *ACS Appl. Mater. Interfaces* **2016**, *8*, 8789–8800. [CrossRef]
10. He, Y.; Jiang, C.Y.; Cao, X.B.; Chen, J.; Tian, W.; Yuan, W.Z. Reducing ice adhesion by hierarchical micro-nano-pillars. *Appl. Surf. Sci.* **2014**, *305*, 589–595. [CrossRef]
11. Meuler, A.J.; McKinley, G.H.; Cohen, R.E. Exploiting topographical texture to impart icephobicity. *ACS Nano* **2010**, *4*, 7048–7052. [CrossRef]
12. Ogawa, K.; Soga, M.; Takada, Y.; Nakayama, I. Development of a transparent and ultrahydrophobic glass plate. *Jpn. J. Appl. Phys.* **1993**, *32*, 614–615. [CrossRef]
13. Kietzig, A.M.; Hatzikiriakos, S.G.; Englezos, P. Patterned superhydrophobic metallic surfaces. *Langmuir* **2009**, *25*, 4821–4827. [CrossRef] [PubMed]
14. Wang, Y.Y.; Li, M.Z.; Lv, T.; Wang, Q.J.; Chen, Q.M.; Ding, J.F. Influence of different chemical modifications on the icephobic properties of superhydrophobic surfaces in a condensate environment. *J. Mater. Chem. A* **2015**, *3*, 4967–4975. [CrossRef]
15. Emelyanenko, A.M.; Boinovich, L.B.; Bezdomnikov, A.A.; Chulkova, E.V.; Emelyanenko, K.A. Reinforced superhydrophobic coating on silicone rubber for longstanding anti -icing performance in severe conditions. *ACS Appl. Mater. Interfaces* **2017**, *9*, 24210–24219. [CrossRef] [PubMed]
16. Guo, P.; Zheng, Y.M.; Wen, M.X.; Song, C.; Lin, Y.C.; Jiang, L. Icephobic/anti-icing properties of micro/nanostructured surfaces. *Adv. Mater.* **2012**, *24*, 2642–2648. [CrossRef]

17. Mishchenko, L.; Hatton, B.; Bahadur, V.; Taylor, J.A.; Krupenkin, T.; Aizenberg, J. Design of ice-free nanostructured surfaces based on repulsion of impacting water droplets. *ACS Nano* **2010**, *4*, 7699–7707. [CrossRef] [PubMed]
18. Wang, L.; Gong, Q.H.; Zhan, S.H.; Jiang, L.; Zheng, Y.M. Robust anti-icing performance of a flexible superhydrophobic surface. *Adv. Mater.* **2016**, *28*, 7729–7735. [CrossRef]
19. Yeong, Y.H.; Wang, C.Y.; Wynne, K.J.; Gupta, M.C. Oil-infused superhydrophobic silicone material for low ice adhesion with long-term infusion stability. *ACS Appl. Mater. Interfaces* **2016**, *8*, 32050–32059. [CrossRef]
20. Wang, Y.L.; Yao, X.; Wu, S.W.; Li, Q.Y.; Lv, J.Y.; Wang, J.J.; Jiang, L. Bioinspired solid organogel materials with a regenerable sacrificial alkane surface layer. *Adv. Mater.* **2017**, *29*, 1700865. [CrossRef] [PubMed]
21. Li, K.Q.; Zeng, X.R.; Li, H.Q.; Lai, X.J. Fabrication and characterization of stable superhydrophobic fluorinated-polyacrylate/silica hybrid coating. *Appl. Surf. Sci.* **2014**, *298*, 214–220. [CrossRef]
22. Xu, W.; An, Q.F.; Hao, L.F.; Huang, L.X. Synthesis, film morphology, and performance of cationic fluorinated polyacrylate emulsion with core-shell structure. *J. Appl. Polym. Sci.* **2012**, *125*, 2376–2383. [CrossRef]
23. Wang, H.; He, G.G.; Tian, Q.Q. Effects of nano-fluorocarbon coating on icing. *Appl. Surf. Sci.* **2012**, *258*, 7219–7224. [CrossRef]
24. Rico, V.; Mora, J.; García, P.; Agüero, A.; Borrás, A.; González-Elipe, A.R.; López-Santos, C. Robust anti-icing superhydrophobic aluminum alloy surfaces by grafting fluorocarbon molecular chains. *Appl. Mater. Today* **2020**, *21*, 100815. [CrossRef]
25. Jia, L.; Sun, J.; Li, X.X.; Zhang, X.; Chen, L.; Tian, X.Y. Preparation and anti-frost performance of PDMS-$SiO_2$/SS superhydrophobic coating. *Coatings* **2020**, *10*, 1051. [CrossRef]
26. Bai, C.Y.; Zhang, X.Y.; Dai, J.B.; Wang, J.H. Synthesis of UV crosslinkable waterborne siloxane-polyurethane dispersion PDMS-PEDA-PU and the properties of the films. *J. Coat. Technol. Res.* **2008**, *5*, 251–257. [CrossRef]
27. Li, X.F.; Zhang, J.F.; Zhou, X.P.; Lu, C.; Tong, X.T.; He, G.X.; Wang, X.Q. Synthesis of core-shell fluoroacrylate copolymer latex via emulsion polymerization and its application in ink-jet ink. *J. Appl. Polym. Sci.* **2012**, *126*, 110–115. [CrossRef]
28. Chen, L.; Zhao, Y.R.; Deng, M.; Yuan, D.X.; Ni, H.G.; Zhang, W.; Wang, X.P. Surface properties and chain structure of fluorinated acrylate copolymers prepared by emulsion polymerization. *Polym. Bull.* **2010**, *64*, 81–97. [CrossRef]
29. Wu, Z.F.; Wang, H.; Tian, X.Y.; Xue, M.; Ding, X.; Ye, X.Z.; Cui, Z.Y. Surface and mechanical properties of hydrophobic silica contained hybrid films of waterborne polyurethane and fluorinated polymethacrylate. *Polymer* **2014**, *55*, 187–194. [CrossRef]
30. Zhang, P.; Lv, F.Y. A review of the recent advances in superhydrophobic surfaces and the emerging energy-related applications. *Energy* **2015**, *82*, 1068–1087. [CrossRef]
31. Cassie, A.B.D.; Baxter, S. Wettability of porous surfaces. *Trans. Faraday Soc.* **1944**, *40*, 546–551. [CrossRef]
32. Wenzel, R.N. Resistance of solid surfaces to wetting by water. *Ind. Eng. Chem.* **1936**, *28*, 988–994. [CrossRef]
33. Wenzel, R.N. Surface roughness and contact angle. *J. Phys. Colloid Chem.* **1949**, *53*, 1466–1467. [CrossRef]
34. Cassie, A.B.D. Contact angles. *Discuss. Faraday Soc.* **1948**, *3*, 11–16. [CrossRef]
35. Chen, J.; Dou, R.M.; Cui, D.P.; Zhang, Q.L.; Zhang, Y.F.; Xu, F.J.; Zhou, X.; Wang, J.J.; Song, Y.L.; Jiang, L. Robust prototypical anti-icing coatings with a self-lubricating liquid water layer between ice and substrate. *ACS Appl. Mater. Interfaces* **2013**, *5*, 4026–4030. [CrossRef]
36. Na, B.; Webb, R.L. A fundamental understanding of factors affecting frost nucleation. *Int. J. Heat Mass Transfer.* **2003**, *46*, 3797–3808. [CrossRef]
37. Miljkovic, N.; Wang, E.N. Condensation heat transfer on superhydrophobic surfaces. *MRS Bull.* **2013**, *38*, 397–406. [CrossRef]
38. Murphy, D.M.; Koop, T. Review of the vapour pressures of ice and supercooled water for atmospheric applications. *Q. J. R. Meteorol. Soc.* **2005**, *131*, 1539–1565. [CrossRef]
39. Boinovich, L.B.; Emelyanenko, A.M.; Emelyanenko, K.A.; Modin, E.B. Modus operandi of protective and anti-icing mechanisms underlying the design of longstanding outdoor icephobic coatings. *ACS Nano* **2019**, *13*, 4335–4346. [CrossRef]